Mid-wave infrared photoluminescence from low-temperature-grown PbSe epitaxial films on GaAs after rapid thermal annealing

Jarod E. Meyer, Leland Nordin, Tri Nguyen, and Kunal Mukherjee[a]

Department of Materials Science and Engineering, Stanford University, Stanford, CA, USA 94305

Abstract

We investigate the beneficial effects of rapid thermal annealing on the structural and photoluminescence properties of PbSe thin films on GaAs (001) grown below 150 °C with a goal of low temperature integration for infrared optoelectronics. Thin films of PbSe deposited on GaAs by molecular beam epitaxy are epitaxial at these reduced growth temperatures, yet the films are highly defective with a mosaic grain structure with low angle and dendritic boundaries following coalescence. Remarkably, we find that rapid thermal annealing for as short as 180 s at temperatures between 300–425 °C in nitrogen ambient leads to extensive re-crystallization and transformation of these grain boundaries. The annealing at the same time dramatically improves the band-edge luminescence at 3.7 μm from previously undetectable levels to nearly half as intense as our best conventionally grown PbSe films at 300 °C. We show using an analysis of laser pump-power dependent photoluminescence measurements that this dramatic improvement in photoluminescence intensity is due to a reduction in the trap-assisted recombination. However, we find it much less correlated to improved structural parameters determined by x-ray diffraction rocking curves, thereby pointing to the elimination of point defects. Overall, the success of rapid thermal annealing in improving the luminescent properties of low growth temperature PbSe is a

[a] Author to whom correspondence should be addressed: kunalm@stanford.edu

step towards the integration of PbSe infrared optoelectronics in low thermal budget, back end of line compatible fabrication processes.

The IV-VI narrow bandgap lead selenide (PbSe) is an attractive material for low-cost mid-wave infrared (MWIR) light emitters[1] in the 3–5 μm range for efficient room temperature operation. Firstly, the bulk nonradiative Auger recombination coefficients of PbSe are 1–2 orders of magnitude lower than bulk narrow bandgap III-V and II-VI semiconductors at room temperature.[2–5] This sets a larger upper bound for internal quantum efficiency (IQE) of light emission in ambient conditions at high injection without the need for complex heterostructure engineering (such as type-II superlattices) to curb Auger losses. Secondly, the high static dielectric constant of PbSe, (ε_s = 210 at 300K) vs. related III-V materials (ε_s = 15 for InAs at 300K) can screen carriers from charged defects and has the potential to impart substantial defect tolerance.[6,7] These attractive properties have led to heteroepitaxial MWIR PbSe lasers and detectors on lattice-mismatched BaF_2 and Si substrates.[8–12] More recently, epitaxial thin films of PbSe on GaAs (001) substrates grown at 300 °C emit photoluminescence (PL) at the band-edge at 3.7 μm with relatively high estimated room temperature IQE.[13] Bright PL was also recently measured in PbSe grown on InAs (111) and 6° offcut Ge (001) substrates.[14,15] Although the optical quality of epitaxial PbSe is excellent when grown at temperatures of roughly 300–400 °C, lower growth and processing temperatures that retain these attractive optical properties may open routes to integration, for example with silicon photonic platforms at back-end-of-line (BEOL) compatible conditions.

A short exposure to higher temperatures in a rapid thermal annealing (RTA) step offers an alternate route to engineering properties while keeping the film deposition to lower temperatures. There are several demonstrations of RTA under inert atmospheres improving the properties of III-V, II-VI, and halide perovskite semiconductors, where a few seconds to a few minutes at elevated

temperatures is sufficient to reduce concentrations of nonradiative recombination centers by defect reactions.[16–20] Annealing studies have primarily been conducted in PbSe in the context of improving detector photosensitivity.[21–23] Longer anneals also control carrier concentrations as deviations from stoichiometry to Pb-rich or Se-rich conditions respectively dope PbSe n- or p-type.[24] Looking at luminescence, Qui et al. found annealing of PbSe films at 380 °C in N_2 and O_2 ambient for 30 minutes to greatly enhance PL, attributed to defect passivation by O_2 and a slight improvement in crystal quality.[22] Zhao et al. also investigated O_2 annealing in 380 °C grown PbSe thin films at temperatures of 150–300 °C for 2 hours and found 200× enhancement in PL intensity,[25] attributed to oxygen passivation of surface recombination. In this work, we grow PbSe thin films by molecular beam epitaxy (MBE) on GaAs(001) substrates at temperatures < 150 ˚C where the film initially has undetectable photoluminescence intensity, and show improved structural and luminescent properties upon RTA processing.

LT-PbSe films were grown by solid source MBE using a Riber C21 system equipped with a compound PbSe effusion cell and a valved cracker Se source. An epi-ready 2" p-type GaAs (001) wafer was degassed at 400 °C in a buffer chamber before being loaded directly into the MBE growth chamber where the native oxide was desorbed at 560 °C under a Se overpressure. Following oxide desorption, the Reflection High Energy Electron Diffraction (RHEED) pattern revealed a diffuse, off-angle streak pattern previously observed in the literature after exposure of GaAs (001) to Se (Figure S1.).[26] The wafer was then exposed to PbSe flux at 400 °C for 30 seconds, which we have previously found important for cube-on-cube epitaxy,[27] though no change in the RHEED pattern was observed. A 10 nm thick PbSe buffer layer was then grown at 330 °C to mediate the 8% lattice-mismatch to GaAs. Substrate manipulator power was then decreased to 0 W and after cooling approximately 300 nm of PbSe was deposited at a growth rate of 0.3 Å/sec.

We estimate the growth temperature of this step is less than 150 °C based on the relationship between thermocouple temperature and the final measured temperature on the MBE optical pyrometer (instrument temperature floor is reached at 250 °C). As observed previously for growth on GaAs (001),[27] PbSe initially grows via a Volmer-Weber island coalescence mode. After full coalescence in roughly 20 nm, the growth mode transitions to layer by layer, and a streaky 1 × 1 was observed in RHEED. The final 10 nm of the PbSe film was doped with Sb for future experiments with metal ohmic contacts but is not studied in this work.

Surface topography of the LT-PbSe film measured by AFM (Park NX-10) reveals an unconventional grain structure shown in Fig. 1a. Only a small fraction of PbSe grain boundaries are oriented along the [100] and [010] directions, corresponding to the low energy nonpolar surfaces of PbSe. Most grains, on the other hand, have no preferred in-plane boundary orientations, possessing a fractal or dendritic-like boundary structure (also referred to as branched growth). Slow adatom diffusion along step edges in comparison to over terraces is often responsible for an instability or roughening that leads to dendrite shaped grain boundaries, commonly seen in 2D materials also grown at low temperatures.[28,29]

Pieces of the LT-PbSe on GaAs wafer were loaded into an RTA chamber (AG associates Heatpulse 210), and proximity-capped with a piece from the same wafer with the PbSe side facing down. Pieces were annealed under N_2 or highly reducing forming gas atmospheres with equivalent results. RTA at 300 °C for 180 s leads to the disappearance of the dendritic grain boundaries, as seen in Fig. 1b. The film undergoing solid-phase recrystallization at higher RTA temperature of 325 °C and the surface develops a texture with facets orienting themselves more sharply with respect to the substrate [110] and [$\bar{1}$10] directions (Fig. 1c). Annealing for 1200 seconds at 325 °C leads to coarsening or an increase in grain size but also significant re-evaporation of the film as

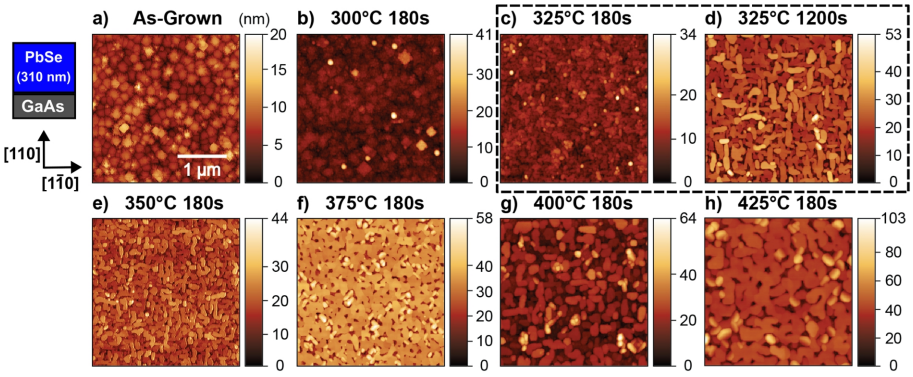

Figure 1. AFM scans of PbSe/GaAs for varying annealing temperatures and times under N_2 ambient. While the LT-PbSe microstructure presents many dendritic grain boundaries **(a)**, annealing at 300 °C for 180 s leads to the disappearance of most grain boundaries **(b)**. Increasing annealing temperatures up to 425 °C **(c, e, f, g, h)** leads to recrystallization aligned with the <110> substrate directions, grain growth, and significant evaporation at higher temperatures. Extending the annealing time at 325 °C to 1200 s leads to more evaporation without as large a change in grain size, compared to the effect of increasing annealing temperature **(c vs. d)**.

evidenced by the greater height variations (Fig. 1d). Continuing this trend, RTA at higher temperatures for 180 s (Figs. 1e–h) yield increasing grain sizes as expected, yet also present a discontinuous microstructure due to film evaporation and potentially limits their use for devices. We note that the RMS roughness increases slightly from 2.2 nm in the LT-PbSe film to 2.7 nm for the film annealed at 325 °C for 180 s, and dramatically increases with annealing temperature to as high as 10.7 nm for the film annealed at 425 °C.

Fig. 2a shows a symmetric 2θ/ω scan of the LT-PbSe film collected using a Panalytical X'Pert PRO MRD system with Cu Kα1 radiation. Only (00*l*)-type PbSe reflections were detected in addition to the substrate, confirming that the film grew single-orientation out-of-plane. A 360° phi-scan of the {224} PbSe and GaAs reflections shown in Fig. 2b, reveals an (001) cube-on-cube epitaxial relationship between the film and substrate. This suggests that the thin 10 nm buffer layer enables epitaxy even at low temperatures. A similar conclusion was reached in the case of PbTe

growth on (111) BaF_2 with RHEED oscillations persisting down to temperatures as low as 95 °C, [30] highlighting the wide epitaxial growth window of this material system.

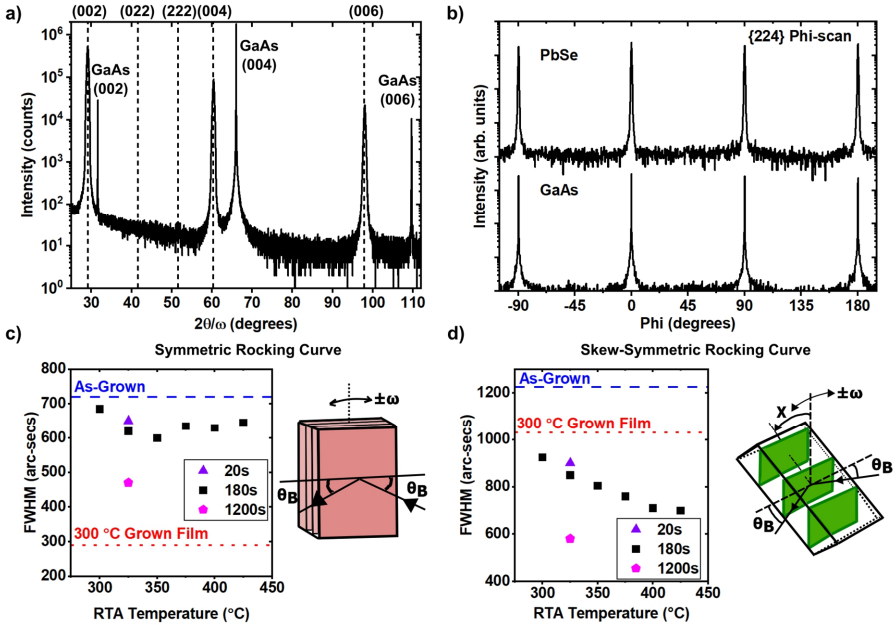

Figure 2. a) Symmetric 2θ/ω scan of as-grown LT-PbSe/GaAs (001) film. The dashed lines show the bulk PbSe peak positions. **b)** 360° phi-scan of the PbSe and GaAs {224} peaks, revealing a cube-on-cube (001) epitaxial relationship. **c)** Symmetric (004) and **d)** Skew-symmetric (224) rocking curve FWHM vs. annealing temperature and time. The dashed and dotted lines show the FWHM of the LT-PbSe sample, and a 300 °C grown sample of similar thickness, respectively. The schematics show the symmetric and skew-symmetric rocking curve geometries.

The dramatic changes in the surface morphology observed for the RTA-processed PbSe films accompanies an improvement in the crystal quality determined by XRD. Fig. 2c shows symmetric, double-axis (004) rocking curves taken for the PbSe films as a function of annealing temperature. The full-width-at-half-maximum (FWHM) of the LT-PbSe sample is broad at 710" when compared to 290" of a baseline PbSe film on GaAs of similar thickness fully grown at 300 °C. RTA for 180 s slightly improves the FWHM to 600" in the best case of 350 °C. Higher temperature anneals led to some degradation. A longer 1200 s anneal reduces the FWHM down to

470", suggesting the crystal quality out-of-plane improves with annealing time but does not surpass the baseline film. Overall, the impact of annealing on the (004) rocking curves is relatively small, but we note that symmetric reflections only capture the out-of-plane tilt disorder and are insensitive to in-plane twist/rotational disorder.[31,32]

Given the clear in-plane reorganization observed with annealing in AFM, skew-symmetric rocking curves of the (224) planes were measured and are shown in Fig. 2d. Surprisingly, the (224) reflection FWHM of both the LT-PbSe and the baseline 300 °C grown film are broad, 1225 and 1030", respectively. Only 180 s of annealing at 300 °C already decreases the (224) FWHM down to 925", with hotter temperatures leading to further reductions in FWHM down to 700" for 425 °C annealing. In the case of longer 1200 s of annealing at 325 °C, the (224) FWHM reduces to 580", well below that of the baseline 300 °C grown film. Thus, the key structural effect of RTA is to improve the in-plane twist disorder of the LT-PbSe film. The capacity of PbSe for such dramatic in-plane reorganization of the grains at modest temperatures complements the recent finding of in-plane and out-of-plane reorientation of grains in PbTe during synthesis on InP.[33] This points to both weak bonding at the PbSe/III-V heterointerface[34] that allows the grains to rotate in-plane and orders of magnitude higher atomic diffusivity of both Pb and Se in PbSe (self-diffusion activation energy 1–2 eV)[35] relative to conventional semiconductors like InAs (self-diffusion activation energy 4–4.5 eV).[36]

From the (224) rocking curves, an estimate of the threading dislocation density (TDD) can be obtained via:[37,38]

$$TDD = \frac{\beta_{224}^2}{4.36b^2} \quad (1)$$

Where b is the burger's vector equal to $\frac{a}{2}[110]$ for PbSe, and β_{224}^2 is the (224) FWHM squared. A TDD of 4.3 × 10^9 cm^{-2} is calculated for the LT-PbSe using Equation 1. Plan-View Electron Channeling Contrast Imaging (ECCI) of the LT-PbSe film reveals a surface TDD of roughly 3.4 × 10^9 cm^{-2} (Figure S2.), in excellent agreement with the XRD result. Applying Equation 1 to the annealed samples suggests that the TDD decreases by no more than a factor of 5, to 1.4 × 10^9 cm^{-}

^{2} in the case of the sample annealed for 180 seconds at 425 °C, and down to 9.7×10^{8} cm^{-2} in the case of the sample annealed for 1200 seconds at 325 °C.

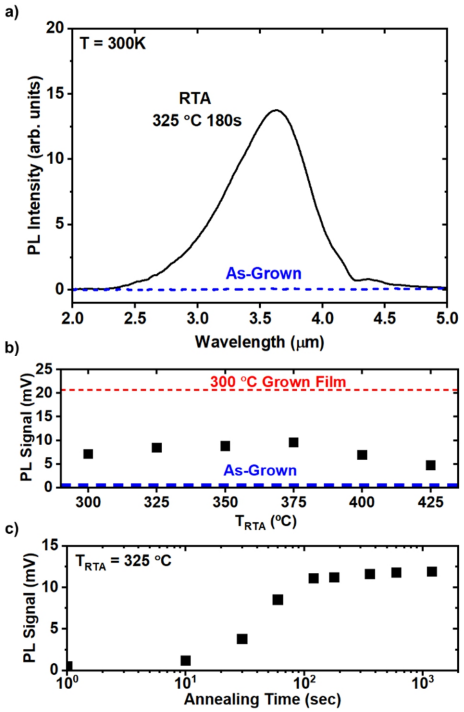

Figure 3. a) Room-temperature, high injection PL spectra of the LT-PbSe sample (blue dashed line), and representative spectra of a sample annealed for 180 seconds at 325 °C. **b)** PL signal vs. annealing temperature for 180 second anneals compared to the LT-PbSe (blue dashed line) and a 300 °C grown film (red dotted line). **c)** PL signal vs. annealing time for a sample progressively annealed at 325 °C.

We measure room temperature high injection and pump-dependent PL to probe the effect of RTA processing on luminescence properties. Quasi-continuous wave PL was measured using an 808 nm laser electrically modulated at 10 kHz. For spectrally integrated measurements, sample luminescence was focused onto a liquid nitrogen cooled MCT detector by a reflective parabolic mirror. For spectrally-resolved measurements, luminescence was directed to a Fourier-transform infrared spectrometer (Bruker Invenio-R) operating in step-scan mode. Fig. 3a shows the nearly

undetectable PL spectra of the LT-PbSe film and a representative spectrum from the sample annealed for 180 s at 325 °C. Strong PL with peak wavelengths of 3.6–3.7 μm is detected for all annealing temperatures. Fig. 3b shows the spectrally integrated PL signal as a function of the RTA temperature for 180 s annealed samples. The PL signal rises with annealing temperature up to 375 °C, before decreasing significantly at higher temperatures of 400–425 °C. This dimming in PL occurs despite the monotonic reduction in (224) FWHM, (and TDD), observed with higher annealing temperatures. At best, the PL intensity of the brightest RTA samples are 2.5× dimmer than a baseline 300 °C grown film. Temperature dependent PL from 80 – 296K of the sample annealed at 375 °C shows similar behavior to 300 °C grown PbSe films in our previous work.[13] PL intensity increases by about 1.5× with cooling to 150 – 225K, but then decreases with further cooling to 80K. The FWHM of PL remains broad at 80K, only decreasing from 63 meV at room temperature to 40 meV (Figure S3). Our previous work placed the peak IQE of a film similar to the baseline sample in the range of 20–30% at room temperature from an analysis of carrier recombination lifetimes.[13] The best RTA samples, then by extension, have IQEs in the range of 10%, still comparable to high temperature grown lattice-matched III-V type-II superlattices at these challenging MWIR wavelengths.[39] Lastly, we progressively anneal a single LT-PbSe sample at 325 °C up to 1200 s as shown in Fig. 3c. Remarkably, the films emit detectable PL intensity within just 10 s of annealing, and the PL intensity essentially plateaus with annealing longer than 100 s. Overall, our results show that RTA processing of PbSe at modest 300–400 °C temperatures can be effective for MWIR emitting devices, circumventing the need for long growths at 300 °C.

Decreasing trap concentration, altered background carrier concentrations, or greater light extraction due to roughness because of the RTA can all result in improved PL. We may distinguish between these possibilities using laser pump power-dependent PL measurements. First, assuming a constant light extraction efficiency, the PL efficiency given by the ratio of integrated PL intensity to incident pump laser power across orders of magnitude of pump excitation power tracks the IQE of light emission as a function of carrier generation rate G.[13,40] By comparing these trends to a model of IQE, we can discriminate between decreasing recombination at traps and altered

background carrier concentration as described below. In the approximation known as the 'ABC' model, the IQE for a n-type semiconductor can be modeled as[41]:

$$IQE = \frac{B(\Delta n + n_0)(\Delta p)}{R_{trap} + B(\Delta n + n_0)(\Delta p) + C_n(\Delta n + n_0)^2(\Delta p) + C_p(\Delta n + n_0)(\Delta p)^2} = \frac{R_{rad}}{G} \quad (2)$$

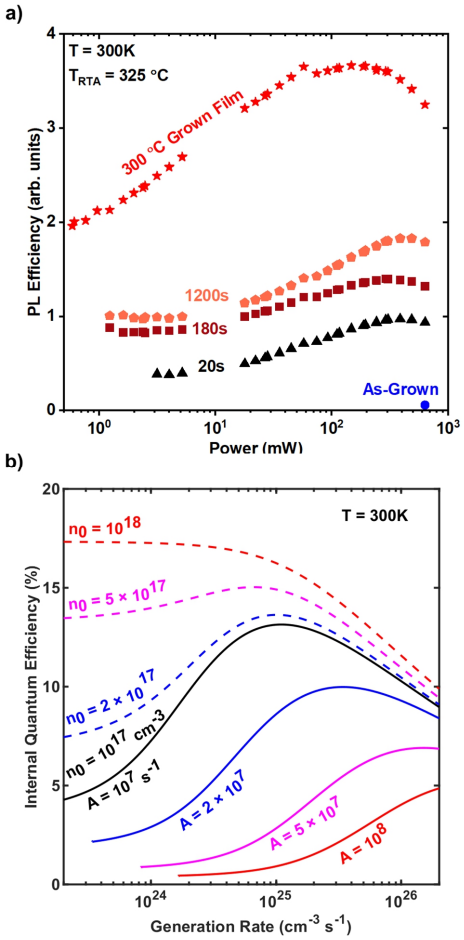

Figure 4. a) Room temperature PL Efficiency vs. laser pump power for LT-PbSe samples annealed at 325C for 20 seconds (triangles), 180 seconds (squares), and 1200 seconds (pentagons), respectively. For comparison, the PL Efficiency of the 300C grown film is plotted (red stars), and an upper bound on the PL Efficiency of the as-grown LT-PbSe film (blue circle). **b)** Modeled IQE curves for PbSe as a function of increasing trap-assisted recombination A coefficients (solid lines) or increasing background carrier concentrations (dashed lines).

Here A, B, C_n, and C_p are the nonradiative trap-assisted, radiative, nonradiative electron-electron-hole Auger and nonradiative hole-hole-electron recombination coefficients, respectively. n_0 is the background electron concentration as we assume the film is n-type because no excess Se was

supplied during growth.[42] Finally, Δn = Δp are the steady-state injected electron and hole carrier densities, and R_{trap} is the trap-assisted recombination rate given as[43]:

$$R_{trap} = \frac{(\Delta n + n_0)\Delta p}{\tau_p(\Delta n + n_0) + \tau_n \Delta p}\ , \tag{3}$$

where τ_n and τ_p are the trap electron and hole lifetimes, respectively. In high injection, R_{trap} reduces to the term $R_{trap} = A\Delta n$ with $A = (\tau_n + \tau_p)^{-1}$.[44] The IQE equals the ratio of the radiative recombination rate R_{rad} to the total recombination rate, the latter being equal to the generation rate in steady state.

Fig. 4a shows room temperature PL efficiency vs. laser pump power for samples annealed at 325 °C for 20, 180, and 1200 s, and compared to the baseline 300 °C grown. The PL efficiency shows the well-known rise and fall as a function of the laser pump power[45] that is reasonably described by the ABC model. Fig. 4b shows the modeled IQE trends as a function of the generation rate starting with the baseline case of an 'A' coefficient of 10^7 s^{-1}, assuming equal electron and hole lifetimes ($\tau_n = \tau_p = 50$ ns, i.e. a trap-assisted recombination lifetime of 100 ns[13]), and $n_0 = 10^{17}$ cm^{-3}. We use B and C_n coefficients for PbSe from the literature[4,46], but we note that the modeling results change little between n- and p-type doping due to the symmetric conduction/valence bands of PbSe. The solid curves in Fig. 4b show the impact of increasing the 'A' coefficient up to 10^8 s^{-1} indicating either more recombination centers or more damaging recombination centers in the sample, while the dashed curves show the impact of increasing background n_0 up to 10^{18} cm^{-3}. As expected, the modeled IQE of PbSe is sensitive to the trap-assisted recombination rate and as the 'A' coefficient is decreased, the low injection IQE increases greatly and the peak IQE shifts to lower carrier generation rates. Finally, at high injection, all IQE curves show droop due to nonradiative Auger recombination.

Comparing Fig. 4a and 4b, the overall increase in PL efficiency observed with RTA time suggests that annealing primarily reduces the density or efficacy of recombination centers. If a change in background doping were responsible for the luminescence enhancement, large changes in the overall shape of the PL efficiency curve would be expected where the low injection IQE

would approach the peak IQE for higher doping concentrations (i.e. no rise in the curve).[41,44] We do not see this and the ratio of the peak PL efficiency to the low injection PL efficiency stays roughly around two for the different annealing times. We think that trap-assisted recombination still limits the annealed films, and beyond a point, the remaining defects no longer anneal out. We speculate that the decrease in PL intensity beyond 400 °C annealing may be due to the evaporation observed in AFM that may enhance recombination at surface sites.

There remain some discrepancies when using the simple ABC model. The slight shift of the peak PL efficiency to higher pump powers for the 1200 s annealed sample is not in line with solely a reduction in the 'A' coefficient. Our assumption of a constant A coefficient with laser pump power,[47] or additional mechanisms like trap-assisted Auger recombination,[48] may be responsible. Finally, we find that annealing the baseline 300 °C grown sample for 180 s at 375 °C hardly improves the high injection PL intensity, at most by 1%, suggesting that changes in light extraction induced from the nm-scale film roughening are negligible.

It is intriguing that the large changes in structural quality and surface morphology between 180 s and 1200 s of annealing at 325 °C only weakly improves the room-temperature PL intensity. Extended defects like dislocations set the FWHM of XRD rocking curves but do not appear to limit the luminescence efficiency. Between 180 and 1200 seconds of annealing at 325 °C, the TDD decreases by roughly a factor of 2. If the low injection PL efficiency was limited by trap assisted recombination at dislocations, the low injection PL efficiency should also rise by roughly a factor of 2, yet only increases by about 20%. Likewise, the low injection PL efficiency increases by almost a factor of 2 between 20 and 180 seconds of annealing at 325 °C, despite a negligible change in structural quality and TDD. Perhaps this tolerance to dislocations allows heteroepitaxial PbSe to function well as a light emitter, and when coupled with a low Auger recombination rate enables even polycrystalline PbSe detectors to efficiently operate at room temperature.[7] Nevertheless, PbSe is not immune to defects as evidenced by the cold-grown PbSe sample having no detectable PL at room temperature. We speculate that the important defects to control for efficient light emission are point defects. Lischka and Prier have measured deep levels in

unintentionally doped PbSe films.[49] Likewise, Brandt et al. note the onset of an impurity band upon electron irradiation of PbSe and PbSnSe samples, tentatively associated with Se vacancies.[50] Our present work highlights the effectiveness of RTA for high optical quality in low-temperature grown PbSe and, importantly, demonstrates the potential for realizing heteroepitaxial PbSe optoelectronic devices in instances where tight thermal budgets are necessary.

We gratefully acknowledge support via the NSF CAREER award under Grant No. DMR-2036520 and the UC Santa Barbara NSF Quantum Foundry funded via the Q-AMASE-I program under Award No. DMR-1906325. Part of this work was performed at the Stanford Nano Shared Facilities (SNSF), supported by the National Science Foundation under Award No. ECCS-2026822. L.N gratefully acknowledges support from the Geballe Laboratory for Advanced Materials postdoctoral research fellowship.

Supplementary Material

See the supplementary material for RHEED of the native oxide desorbed GaAs surface under Se atmosphere, ECCI of the LT-PbSe film, and temperature dependent photoluminescence spectra.

Author declarations

Conflict of interest

The authors have no conflicts to disclose.

Data Availability

The data that supports the findings of this study are available from the corresponding author upon reasonable request.

References

[1] D. Jung, S. Bank, M.L. Lee, and D. Wasserman, "Next-generation mid-infrared sources," J. Opt. **19**(12), 123001 (2017).
[2] R. Klann, T. Höfer, R. Buhleier, T. Elsaesser, and J.W. Tomm, "Fast recombination processes in lead chalcogenide semiconductors studied via transient optical nonlinearities," Journal of Applied Physics **77**(1), 277–286 (1995).
[3] P.C. Findlay, C.R. Pidgeon, R. Kotitschke, A. Hollingworth, B.N. Murdin, C.J.G.M. Langerak, A.F.G. van der Meer, C.M. Ciesla, J. Oswald, A. Homer, G. Springholz, and G. Bauer, "Auger recombination dynamics of lead salts under picosecond free-electron-laser excitation," Phys. Rev. B **58**(19), 12908–12915 (1998).
[4] X. Zhang, J.-X. Shen, and C.G. Van de Walle, "Anomalous Auger Recombination in PbSe," Phys. Rev. Lett. **125**(3), 037401 (2020).
[5] J.R. Meyer, C.L. Canedy, M. Kim, C.S. Kim, C.D. Merritt, W.W. Bewley, and I. Vurgaftman, "Comparison of Auger Coefficients in Type I and Type II Quantum Well Midwave Infrared Lasers," IEEE J. Quantum Electron. **57**(5), 1–10 (2021).
[6] R.S. Allgaier, and W.W. Scanlon, "Mobility of Electrons and Holes in PbS, PbSe, and PbTe between Room Temperature and 4.2K," Phys. Rev. **111**(4), 1029–1037 (1958).
[7] G. Springholz, and G. Bauer, in *Wiley Encyclopedia of Electrical and Electronics Engineering* (John Wiley & Sons, 2014), pp. 1–16.
[8] H. Zogg, and M. Hüppi, "Growth of high quality epitaxial PbSe onto Si using a (Ca,Ba)F $_2$ buffer layer," Appl. Phys. Lett. **47**(2), 133–135 (1985).
[9] P.J. McCann, X.M. Fang, W.K. Liu, B.N. Strecker, and M.B. Santos, "MBE growth of PbSe/CaF2/Si(1 1 1) heterostructures," Journal of Crystal Growth **175–176**, 1057–1062 (1997).
[10] H. Zogg, "Photovoltaic lead-chalcogenide on silicon infrared sensor arrays," Opt. Eng **33**(5), 1440 (1994).
[11] Z. Shi, G. Xu, P.J. McCann, X.M. Fang, N. Dai, C.L. Felix, W.W. Bewley, I. Vurgaftman, and J.R. Meyer, "IV–VI compound midinfrared high-reflectivity mirrors and vertical-cavity surface-emitting lasers grown by molecular-beam epitaxy," Appl. Phys. Lett. **76**(25), 3688–3690 (2000).
[12] M. Fill, A. Khiar, M. Rahim, F. Felder, and H. Zogg, "PbSe quantum well mid-infrared vertical external cavity surface emitting laser on Si-substrates," Journal of Applied Physics **109**(9), 093101 (2011).
[13] J. Meyer, A.J. Muhowski, L. Nordin, E. Hughes, B. Haidet, D. Wasserman, and K. Mukherjee, "Bright mid-infrared photoluminescence from high dislocation density epitaxial PbSe films on GaAs," APL Materials **9**(11), 111112 (2021).
[14] B.B. Haidet, L. Nordin, A.J. Muhowski, K.D. Vallejo, E.T. Hughes, J. Meyer, P.J. Simmonds, D. Wasserman, and K. Mukherjee, "Interface structure and luminescence properties of epitaxial PbSe films on InAs(111)A," Journal of Vacuum Science & Technology A **39**(2), 023404 (2021).
[15] L.L. McDowell, J. Qiu, M.R. Mirzaei, B. Weng, and Z. Shi, "Integration of Epitaxial IV–VI Pb-Chalcogenide on Group IV Vicinal Ge Substrate to Form p–n Heterogeneous Structures," Crystal Growth & Design **22**(1), 461–468 (2022).
[16] N. Chand, R. People, F.A. Baiocchi, K.W. Wecht, and A.Y. Cho, "Significant improvement in crystalline quality of molecular beam epitaxially grown GaAs on Si (100) by rapid thermal annealing," Appl. Phys. Lett. **49**(13), 815–817 (1986).

[17] J.C. Zolper, M. Hagerott Crawford, A.J. Howard, J. Ramer, and S.D. Hersee, "Morphology and photoluminescence improvements from high-temperature rapid thermal annealing of GaN," Appl. Phys. Lett. **68**(2), 200–202 (1996).
[18] M.D. Kim, M.S. Han, T.W. Kang, and T.W. Kim, "Effect of thermal annealing on the structural and optical properties of CdTe (111)/GaAs (100) heterostructures," Thin Solid Films **310**(1–2), 132–137 (1997).
[19] T. Kageyama, T. Miyamoto, S. Makino, F. Koyama, and K. Iga, "Thermal Annealing of GaInNAs/GaAs Quantum Wells Grown by Chemical Beam Epitaxy and Its Effect on Photoluminescence," Jpn. J. Appl. Phys. **38**(3B), L298 (1999).
[20] V.L. Pool, B. Dou, D.G. Van Campen, T.R. Klein-Stockert, F.S. Barnes, S.E. Shaheen, M.I. Ahmad, M.F.A.M. van Hest, and M.F. Toney, "Thermal engineering of FAPbI3 perovskite material via radiative thermal annealing and in situ XRD," Nat Commun **8**(1), 14075 (2017).
[21] F. Briones, D. Golmayo, and C. Ortiz, "The role of oxygen in the sensitization of photoconductive PbSe films," Thin Solid Films **78**(4), 385–395 (1981).
[22] J. Qiu, B. Weng, Z. Yuan, and Z. Shi, "Study of sensitization process on mid-infrared uncooled PbSe photoconductive detectors leads to high detectivity," Journal of Applied Physics **113**(10), 103102 (2013).
[23] N.A. Tret'yakova, "Study of heat-sensitization modes of lead selenide films prepared by hydrochemical synthesis," J. Synch. Investig. **8**(4), 632–635 (2014).
[24] N. Ôhashi, and K. Igaki, "Physico-Chemical Study on Lead Selenide," Trans. JIM **5**(2), 94–96 (1964).
[25] F. Zhao, S. Mukherjee, J. Ma, D. Li, S.L. Elizondo, and Z. Shi, "Influence of oxygen passivation on optical properties of PbSe thin films," Appl. Phys. Lett. **92**(21), 211110 (2008).
[26] H. Abe, K. Ueno, K.S. Koichiro Saiki, and A.K. Atsushi Koma, "Heteroepitaxial Growth of Layered GaSe Films on GaAs(001) Surfaces," Jpn. J. Appl. Phys. **32**(10A), L1444 (1993).
[27] B.B. Haidet, E.T. Hughes, and K. Mukherjee, "Nucleation control and interface structure of rocksalt PbSe on (001) zincblende III-V surfaces," Phys. Rev. Materials **4**(3), 033402 (2020).
[28] L. Jiao, H.J. Liu, J.L. Chen, Y. Yi, W.G. Chen, Y. Cai, J.N. Wang, X.Q. Dai, N. Wang, W.K. Ho, and M.H. Xie, "Molecular-beam epitaxy of monolayer MoSe $_2$: growth characteristics and domain boundary formation," New J. Phys. **17**(5), 053023 (2015).
[29] R. Yue, Y. Nie, L.A. Walsh, R. Addou, C. Liang, N. Lu, A.T. Barton, H. Zhu, Z. Che, D. Barrera, L. Cheng, P.-R. Cha, Y.J. Chabal, J.W.P. Hsu, J. Kim, M.J. Kim, L. Colombo, R.M. Wallace, K. Cho, and C.L. Hinkle, "Nucleation and growth of WSe $_2$: enabling large grain transition metal dichalcogenides," 2D Mater. **4**(4), 045019 (2017).
[30] G. Springholz, and G. Bauer, "Low temperature growth of PbTe and of PbTe/Pb1−xEuxTe multi-quantum wells by molecular beam epitaxy," Journal of Crystal Growth **144**(3–4), 157–172 (1994).
[31] V. Srikant, J.S. Speck, and D.R. Clarke, "Mosaic structure in epitaxial thin films having large lattice mismatch," Journal of Applied Physics **82**(9), 4286–4295 (1997).
[32] B. Heying, X.H. Wu, S. Keller, Y. Li, D. Kapolnek, B.P. Keller, S.P. DenBaars, and J.S. Speck, "Role of threading dislocation structure on the x-ray diffraction peak widths in epitaxial GaN films," Appl. Phys. Lett. **68**(5), 643–645 (1996).
[33] J. Jung, S.G. Schellingerhout, O.A.H. van der Molen, W.H.J. Peeters, M.A. Verheijen, and E.P.A.M. Bakkers, "Single-crystalline PbTe film growth through reorientation," Phys. Rev. Mater. **7**(2), 023401 (2023).

[34] B.B. Haidet, J. Meyer, P. Reddy, E.T. Hughes, and K. Mukherjee, "Versatile strain relief pathways in epitaxial films of (001)-oriented PbSe on III-V substrates," Phys. Rev. Mater. **7**(2), 024602 (2023).
[35] R.L. Guldi, J.N. Walpole, and R.H. Rediker, "Diffusion of lead and selenium in lead selenide," Journal of Applied Physics **44**(11), 4896–4907 (1973).
[36] A.F.W. Willoughby, "Self-Diffusion in Compound Semiconductors," MRS Online Proceedings Library **14**(1), 237–252 (1982).
[37] J.E. Ayers, "The measurement of threading dislocation densities in semiconductor crystals by X-ray diffraction," Journal of Crystal Growth **135**(1–2), 71–77 (1994).
[38] M.J. Hordon, and B.L. Averbach, "X-ray measurements of dislocation density in deformed Copper and Aluminum single crystals," Acta Metallurgica **9**(3), 237–246 (1961).
[39] A.J. Muhowski, A.M. Muellerleile, J.T. Olesberg, and J.P. Prineas, "Internal quantum efficiency in 6.1 Å superlattices of 77% for mid-wave infrared emitters," Appl. Phys. Lett. **117**(6), 061101 (2020).
[40] C.H. Swartz, K.N. Zaunbrecher, S. Sohal, E.G. LeBlanc, M. Edirisooriya, O.S. Ogedengbe, J.E. Petersen, P.A.R.D. Jayathilaka, T.H. Myers, M.W. Holtz, and T.M. Barnes, "Factors influencing photoluminescence and photocarrier lifetime in CdSeTe/CdMgTe double heterostructures," Journal of Applied Physics **120**(16), 165305 (2016).
[41] S. Karpov, "ABC-model for interpretation of internal quantum efficiency and its droop in III-nitride LEDs: a review," Opt Quant Electron **47**(6), 1293–1303 (2015).
[42] D.K. Hohnke, and S.W. Kaiser, "Epitaxial PbSe and Pb $_{1-x}$ Sn $_{x}$ Se: Growth and electrical properties," Journal of Applied Physics **45**(2), 892–897 (1974).
[43] R.N. Hall, "Electron-Hole Recombination in Germanium," Phys. Rev. **87**(2), 387–387 (1952).
[44] B. Galler, H.-J. Lugauer, M. Binder, R. Hollweck, Y. Folwill, A. Nirschl, A. Gomez-Iglesias, B. Hahn, J. Wagner, and M. Sabathil, "Experimental Determination of the Dominant Type of Auger Recombination in InGaN Quantum Wells," Appl. Phys. Express **6**(11), 112101 (2013).
[45] A.W. Walker, S. Heckelmann, C. Karcher, O. Höhn, C. Went, M. Niemeyer, A.W. Bett, and D. Lackner, "Nonradiative lifetime extraction using power-dependent relative photoluminescence of III-V semiconductor double-heterostructures," Journal of Applied Physics **119**(15), 155702 (2016).
[46] H. Zogg, W. Vogt, and W. Baumgartner, "Carrier recombination in single crystal PbSe," Solid-State Electronics **25**(12), 1147–1155 (1982).
[47] F. Zhang, J.F. Castaneda, T.H. Gfroerer, D. Friedman, Y.-H. Zhang, M.W. Wanlass, and Y. Zhang, "An all optical approach for comprehensive in-operando analysis of radiative and nonradiative recombination processes in GaAs double heterostructures," Light Sci Appl **11**(1), 137 (2022).
[48] A. David, N.G. Young, C.A. Hurni, and M.D. Craven, "Quantum Efficiency of III-Nitride Emitters: Evidence for Defect-Assisted Nonradiative Recombination and its Effect on the Green Gap," Phys. Rev. Applied **11**(3), 031001 (2019).
[49] K. Lischka, and H. Preier, "Observation of Localized Deep Levels in PbSe," Phys. Stat. Sol. (b) **101**(2), K129–K134 (1980).
[50] N.B. Brandt, B.B. Kovalev, and E.P. Skipetrov, "Pressure studies of the energy spectrum of irradiation-induced defects in Pb $_{1-x}$ Sn $_{x}$ Se," Semicond. Sci. Technol. **6**(6), 487–490 (1991).